Distributed Acoustic Sensing to Monitor Ground Motion/Movement at Multi-Frequency Bands

Xin Lu, Konstantin Hicke, and Katerina Krebber

***Abstract*—A novel distributed acoustic sensing technique is proposed that exploits both phase and amplitude of the Rayleigh backscattered light to quantify the environmental variation. The system employs a wavelength-scanning laser and an imbalanced Mach-Zehnder interferometer to acquire the reflection spectra and the phase of the detected light, respectively. Fading-free and low-frequency measurements are realized via the cross-correlation of the reflection spectra. The discrete cross-correlation is used to circumvent the nonlinear frequency sweeping of the laser. Based on the phase of the backscattered light, it is possible to quantify fast environmental variations. The whole system requires no hardware modification of the existing system and its functionality is experimentally validated. The proposed system has the potential to monitor ground motion/movement at very low frequency band like subsidence around mining areas and at high frequency band like earthquakes and vibrations induced by avalanches.**

***Index Terms*—Distributed acoustic sensing, ground motion, ground movement, optical fiber sensing, Rayleigh fading.**

I. Introduction

GROUND motion/movement can be considered as any change of the ground surface or the strata in horizontal and/or vertical direction. It can be a natural event, such as an earthquake, or be related to human activities, e.g., subsidence caused by mining. All these events occur at different frequencies and different strengths. More importantly, they have usually a destructive impact on our society and the ecosystem. For example, a strong ground motion/movement may cost lives and undermine the integrity of infrastructures. In order to avoid hazardous consequences, the ground motion/movement should be closely monitored around the clock over large areas.

Phase-sensitive optical time domain reflectometry (φOTDR), as a distributed acoustic sensing (DAS) technique, is an excellent candidate for ground motion/movement due to its simple configuration and high performance [1]. The φOTDR system launches coherent pulses into the sensing fiber and collects the interference of light backscattered at the inhomogeneities inside the fiber as a function of time. In this way, spatially-resolved measurements can be realized and the system exhibits a very high sensitivity thanks to the interference process [1]. The φOTDR system has been successfully commercialized in the last decade and applied to detect various ground motions/movements, such as seismic events [2], landslides [3], etc.

When the fiber is subject to environmental variations, the interference condition of the backscattered light is modified, so the obtained signal changes accordingly. The φOTDR system can only locate the perturbation and retrieve the frequency in its infancy. After about 30 years development, various methods have been proposed to quantify the environmental variation, particularly vibration, using the amplitude or phase of the detected signal [1], named as the amplitude-based method (ABM) and phase-based method (PBM), respectively. Wavelength-scanning φOTDR is one type of the amplitude-based systems, it uses the reflection spectrum shift, which is obtained usually by cross-correlation of the local spectra of two measurements, to retrieve the local environmental change for static and dynamic measurements [4], [5]. Another ABM determines the external perturbation by the temporal correlation of the φOTDR traces obtained with a frequency chirped pulse [6]. The environmental changes also introduce a phase delay of the backscattered light. Thus, the PBM relies on the optical phase to quantify the environmental change [7], [8].

In spite of the great success and remarkable development in the past years, different types of the φOTDR systems have their own intrinsic drawbacks. Although the φOTDR based on frequency scanning (an amplitude-based method) demonstrates an excellent performance at low frequency and can measure quasi-DC signals [5], its maximum measurable frequency is greatly limited by the scanning speed. Moreover, extra and sophisticated equipment is needed to realize the linear frequency scanning [9], [10]. Although directly modulating the driving current of the laser is a simple solution to frequency scanning, the frequency change is usually not linear, causing problem for data processing [4]. The chirped-pulse φOTDR, as another ABM, can reach the high frequency limited by the sensing distance, it however requires sophisticated equipment and a large detection bandwidth, increasing the cost and introducing more noise since the dominant noise in the system is proportional to the bandwidth [11]. The PBM is able to perform high frequency measurements, but it mostly suffers from the fading effect, to which the amplitude-based system is intrinsically immune. In addition, the redistribution of the inhomogeneity under perturbation will introduce a random phase variance, which results in low-frequency noise, causing problems for the low frequency measurement [12]. As

Manuscript received 6 December 2023; revised 13 January 2024; accepted 21 January 2024. Date of publication 25 January 2024; date of current version 16 September 2024. *(Corresponding author: Xin Lu.)*

The authors are with the Bundesanstalt für Materialforschung und -prüfung (BAM), Unter den Eichen 87, 12205 Berlin, Germany (e-mail: xin.lu@bam.de; konstantin.hicke@bam.de; katerina.krebber@bam.de).

Color versions of one or more figures in this article are available at https://doi.org/10.1109/JLT.2024.3358495.

Digital Object Identifier 10.1109/JLT.2024.3358495

a result, it is still challenging for a single φOTDR system to simultaneously measure environmental variations at high and low frequencies.

To answer to the current challenge, the amplitude- and phase-based methods can be combined in a single φOTDR system, so that the system can cover multi-frequency bands, as the ABM and PBM quantify the environmental changes at low and high frequency ranges, respectively [13]. Such a φOTDR system is proposed in this paper, which is essentially the same as the phase-based system using an imbalanced Mach-Zehnder interferometer (IMZI) and three photodetectors [14], [15], but the optical frequency from the light source is modulated by a ramp signal, so that the proposed system can also work as the wavelength scanning φOTDR. As a result, the new system becomes multi-functional and is able to perform several tasks simultaneously. The optical phase can be retrieved in the system via the IMZI scheme, enabling high-frequency sensing. The cross-correlation of the obtained amplitude enables fading-free low-frequency measurements. A discrete correlation function is employed to circumvent the problem of the nonlinear scanning. All the functionalities of the proposed system have been successfully demonstrated by experiments over a 1.4 km long fiber.

II. Working Principles of the Proposed Method

A. φOTDR With the IMZI Scheme

The optical fiber is not perfectly uniform and actually consists of enormous inhomogeneities. The incident light is scattered at the inhomogeneity and a small portion of the scattered light travels back to the fiber entrance. The light backscattered within the half length of the optical pulse superposes each other at the photodetector, equivalent to an interference process, so the obtained signal is dependent on the local fiber condition, which is subject to the environmental change. When the corresponding fiber section experiences external perturbations, the signal changes accordingly. For example, the refractive index and the interval amongst the inhomogeneities change if the fiber is stretched, resulting in an optical phase delay. The PBM aims to reconstruct the optical phase of the backscattered light in order to quantify the environmental change.

The PBM can be realized by coherent or direct detection in a φOTDR system. For the former detection method, the optical phase is usually obtained by the IQ demodulation of the beat between the backscattered light and a local oscillator [7], [8]. Note that the obtained phase accumulates along the fiber, and it is prone to the phase noise from the laser. Moreover, a local environmental change introduces a phase delay to the light backscattered after that position. To suppress all these influences, the phase difference of two positions is usually used instead of the absolute value. For example, the phase difference between the two dotted areas in Fig. 1(a) reveals the environmental condition from z to $z + \Delta l$.

The φOTDR based on direct detection on the other hand usually needs an interferometer to encode the phase information into amplitude of the light. The IMZI is such a scheme, it consists of a 1:2 splitter and a 3 × 3 coupler as shown in Fig. 1(b). The light backscattered from the sensing fiber is at first evenly

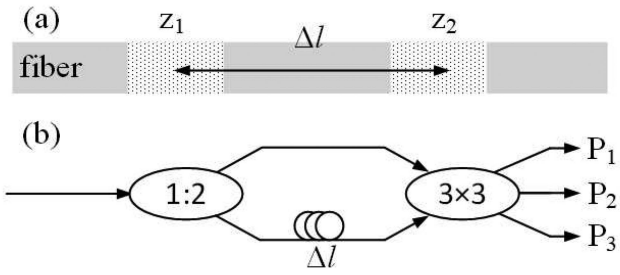

Fig. 1. (a) The phase difference between two positions determines the environmental condition, (b) schematic diagram of the imbalanced Mach–Zehnder interferometer used for phase retrieval.

separated by the splitter. Then the split lightwaves travel through different arms of the interferometer and recombine at the 3 × 3 coupler. The outputs of the coupler connect directly to three identical photodetectors to acquire the signal. Since the lengths of the arms are different, the light traveling in one arm is delayed by a length of Δl compared with the other one. Consequently, the output of the coupler is dependent not only on the amplitude of the backscattered light, but also on the optical phase difference $\Delta\varphi$ between two fiber positions. The phase difference between two positions with an interval of Δl in Fig. 1(a) can be expressed as [16]

$$\Delta\varphi\left(z,t\right)=4\pi n\Delta l\nu/c+\varphi'\left(z+\Delta l,t\right)-\varphi'\left(z,t\right) \tag{1}$$

where n is the refractive index of the fiber, ν is the optical frequency, c is the light speed in vacuum, $\varphi'(z)$ and $\varphi'(z+\Delta l)$ are random phases from the dotted section as shown in Fig. 1(a). The first term on the right-hand side of (1) is believed to change linearly with temperature and strain, the other terms however vary randomly owing to the random relocation of the inhomogeneities due to the environmental change. The phases accumulate during the measurement time, resulting in a low-frequency noise [12]. The performance of the phase-based φOTDR system is consequently undermined.

There exist two signal demodulation methods to retrieve the optical phase difference for the φOTDR system with the IMZI scheme: IQ demodulation and differentiation and cross multiply (DCM). The differentiation step in the DCM algorithm is more prone to noise [15], so the IQ demodulation is used here. Based on the signals obtained by the photodetectors, in-phase sig_I and quadrature sig_Q components can be computed as [1], [15], [17]:

$$\begin{cases} sig_I\left(z,t\right)=-P_1\left(z,t\right)/2+P_2\left(z,t\right)-P_3\left(z,t\right)/2 \\ sig_Q\left(z,t\right)=-\sqrt{3}P_1\left(z,t\right)/2+\sqrt{3}P_3\left(z,t\right)/2 \end{cases} \tag{2}$$

where P_i $(i=1,2,3)$ are the signals from the three photodetectors. Detailed derivation of the signal and the IQ demodulation can be found in supplement A. Then the amplitude A_{de} and the phase difference $\Delta\varphi$ can be obtained

$$\begin{cases} A_{de}\left(z,t\right)\propto\sqrt{sig_I^2\left(z,t\right)+sig_Q^2\left(z,t\right)} \\ \Delta\varphi\left(z,t\right)\approx\arctan\left[sig_Q\left(z,t\right)/sig_I\left(z,t\right)\right] \end{cases} \tag{3}$$

The arc-tangent function only provides a phase range from $-\pi/2$ to $\pi/2$. Thus, phase unwrapping is usually necessary to

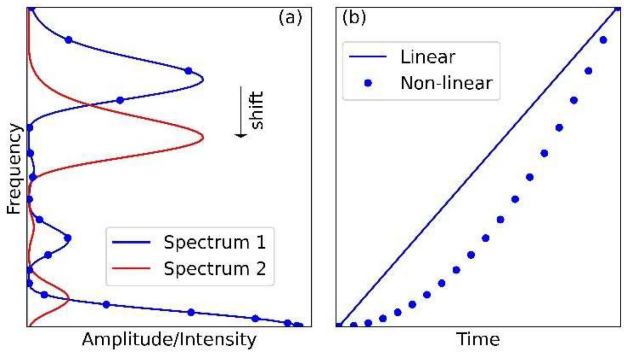

Fig. 2. (a) Reflection spectra (change of optical intensity as a function of optical frequency) at a given position before and after an environmental condition change. (b) Illustration of the laser frequency change over time, which is usually non-linear during the scanning.

expand the value of the demodulated phase $\Delta\varphi$, and the environmental information can be obtained from the unwrapped phase based on the pre-determined relationship. For example, 1 $\mu\varepsilon$ strain over 1 m fiber causes a phase change of ~9.2 rad when the incident light is at 1550 nm [18].

The obtained φOTDR signal exhibits a well-known stochastic profile along the fiber due to the random interference, so the received signal can be very low at many positions, named as fading. Many literatures have reported the relationship between the error of the demodulated phase and the local signal, i.e., the amplitude of the backscattered light, revealing that the phase error increases greatly at the fading points [17], [19]. For the IMZI based φOTDR system, the demodulated amplitude A_{de} is a good indicator to evaluate the quality of the obtained phase difference [17], [20].

Note that the amplitude obtained by (3) is essentially proportional to the product of $A^2(z)$ and $A^2(z+\Delta l)$ of the backscattered light [17]. External perturbations can change the value of $A^2(z)$ and $A^2(z+\Delta l)$, so the demodulated amplitude A_{de} varies accordingly, which can be used to quantify the perturbation by the frequency scanning φOTDR as explained in the next section.

B. Optical Frequency Scanning φOTDR With the IMZI Scheme

As stated above, the optical fiber is not perfectly uniform; it instead consists of enormous inhomogeneities whose size and density change randomly along the optical fiber, leading to a stochastic profile of the refractive index in the longitudinal direction. As a result, the optical fiber can be considered as a long and weak fiber Bragg grating (FBG) with random periods [9], [21]. A standard FBG can be used to retrieve the environmental information from the reflection spectrum shift of the grating [22]. The wavelength scanning φOTDR system shares the same working principle. The optical frequency of the incident light is scanned within a certain range during the measurement and the reflection spectrum at a given point can be obtained by recording the backscattered light as a function of the scanned frequency. The obtained spectrum will shift if this part of fiber is subject to temperature or strain change, just like the FBG. An example is shown in Fig. 2(a), the blue and red curves represent the reflection spectra before and after the environmental change at a given position, respectively. It is clear that the spectrum shifts along the frequency axis due to the change.

The restorability of the φOTDR trace is another explanation to the working principle [23]. The shape of the temporal trace is essentially the result of an interference process, so it is dependent on the local refractive index, the interval amongst the inhomogeneities and the optical frequency of the incident light. The environmental variation can modify the shape via changing the refractive index and the interval. However, the influence of the environmental change can be compensated by tuning the optical frequency so that the modified trace is restored to its original shape. In this way, the environmental information can be calibrated from the optical frequency shift.

Cross-correlation of the reflection spectra is the standard method to determine the frequency shift [5]. At a given position, the correlation coefficient of the spectra obtained at different measurement times is computed as

$$coef\,(z,t,f) = \frac{\sum_{i=0}^{k}\left[I\,(z,t_0,\nu)-\overline{I}\,(z,t_0)\right]\left[I\,(z,t,\nu+f)-\overline{I}\,(z,t)\right]}{\sqrt{\sum_{i=0}^{k}\left[I\,(z,t_0,\nu)-\overline{I}\,(z,t_0)\right]^2}\sqrt{\sum_{i=0}^{k}\left[I\,(z,t,\nu)-\overline{I}\,(z,t)\right]^2}} \tag{4}$$

where I represent the measured optical intensity/amplitude, the overbar above I denotes the average value of the spectrum, ν is the optical frequency, f is a variable that represent the frequency change and it is the multiple of the frequency scanning step, k is the number of sampling points for a reflection spectrum, subscript 0 denotes the reference measurement. The obtained coefficient changes as a function of f, and the optical frequency shift is determined by the location of the correlation peak that represents the maximum value of the coefficient. The description above reveals that the frequency scanning φOTDR retrieves environmental information by comparing the shape of two spectra. This unique working principle makes it intrinsically immune to fading effect. Furthermore, the obtained spectral shift is dependent only on the light backscattered from the relevant region, unlike the PBM that is influenced by the light from the boundary (the dotted area shown in Fig. 1(a)). This method is therefore less prone to the low frequency noise.

In this paper, the demodulated amplitude A_{de} and its corresponding average value replace I and $\overline{I}$ in (4). A_{de} is equivalent to the product of the reflection spectra at two different positions. The two spectra can be considered as independent because they originate from two positions with an interval that is longer than the pulse width. As a result, their product also shifts due to environmental changes in spectral domain, making it possible to quantify the change. In other words, this spectrum is constructed by plotting the demodulated amplitude as a function of the scanning frequency, and it shifts due to the environmental variation. The frequency shift of this spectrum is determined by (4) and is used to quantify the variation.

Due to the random interference, the reflection spectrum obtained by a φOTDR system has an irregular shape as shown in Fig. 2(a) and the shape changes at every position, depending on the local interference condition. It is consequently possible

that the spectrum reconstructed by the demodulated amplitude is distorted and loses the correlation after the environmental change. A high correlation of the spectra can be maintained if the shape is just a smooth and simple curve without large variation, which can be realized from two aspects. On one hand, the optical pulses should be as narrow as possible. As the correlation frequency of the φOTDR signal is inversely proportional to the pulse width [24], the spectrum obtained with a narrow incident pulse exhibits a simpler shape than with the long pulse within the same frequency scanning range. On the other hand, the scanning range should be small to obtain a simple spectrum shape. These settings match well with the requirement of subsidence monitoring. If the requirement cannot be fulfilled, a small environmental change can result in total distortion of the spectrum based on the demodulated amplitude. Consequently, the spectra before and after the environmental change are no longer correlated, so the correlation peak obtained by (4) vanishes, making it impossible to determine the actual frequency shift.

RF modulation of the incident light is usually used to realize linear frequency scanning, which requires expensive and sophisticated equipment [9], [10]. An economical solution is to directly modulate the driving current of the laser by applying a ramp wave. However, various experiments have demonstrated that the laser frequency usually changes non-linearly with the applied current [4], as illustrated by the dotted line in Fig. 2(b).

Due to this non-linear change of the laser frequency, the scanning step is not constant during the measurement. This leads to a consequence that the reflection spectrum is not evenly sampled, as demonstrated by the dots in Fig. 2(a), causing problem for the cross-correlation. In this case, only the signal obtained at a quasi-linear scanning range is selected to construct the spectrum. For example, the spectrum can be interpolated to reconstruct an equally sampled curve for the cross-correlation [4]. The random interference process however leads to a spectrum with a stochastic profile; thus, the interpolated result becomes less accurate, making the determined frequency shift unreliable. An evenly sampled spectrum can also be built by using neural networks [25], but it requires enormous data and time to train the model. Current methods waste the nonnegligible amount of the data obtained at the nonlinear frequency range.

The cross-correlation of unevenly sampled signal is actually a common problem in many fields, such as economy, geophysics and astronomy [26]. Various approaches have been proposed so far to solve this problem, one of them is called discrete cross-correlation (DCC) [27], [28]. The DCC method consists of three steps. In the first step, the curves to be correlated, which are the spectra based on the demodulated amplitude in this paper, are divided into segments with a uniform width, as the shaded area shown in Fig. 3. Each area covers several sampling points of the curve. Note that the number of sampling points within the segment is not required to be the same. A data pair is formed by selecting one sampling point from each curve within one segment. Then the correlation value (CV) for one pair is calculated for each segment as shown in (5) shown at the bottom of next page, where k and g represent the number of sampling points within the segments for the two spectra, respectively, σ

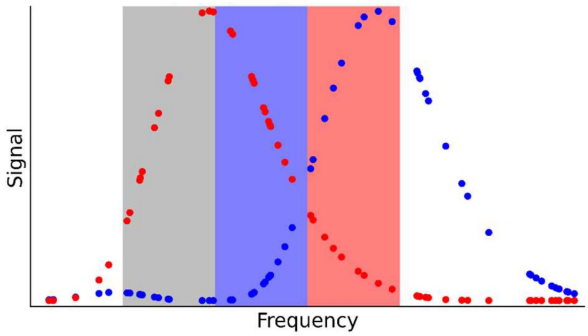

Fig. 3. Uniform segmentation of the curves for the discrete cross-correlation.

denotes the standard deviation of the spectrum in the segment. The third step is to calculate the average of the correlation values obtained for all the pairs within the segment. The operation is repeated to obtain the average for all the segment, and the frequency shift is determined by the location of the largest value. All the obtained data is used to construct the spectrum and the DCC delivers trustworthy result as this method has been tested in many fields for a long time.

III. Experiment and Results

A. Experimental Setup

A configuration of the proposed φOTDR is depicted in Fig. 4. The light source is a high-performance semiconductor laser working at 1550 nm with a very narrow linewidth of a few kHz. The optical frequency of the laser is modulated by a ramp signal from an arbitrary waveform generator (AWG) to realize frequency scanning. The frequency scanning range is controlled by the voltage of the applied signal, and it is set to a small value in order to measure small strain changes, with the aim to monitor subsidence in practice. Based on the IMZI scheme, the scanning range is measured to be about 637 MHz. The output of the laser is gated into pulses by a semiconductor optical amplifier (SOA) which is supposed to achieve a high extinction ratio of $\sim$70 dB. The generated pulses are amplified by an erbium-doped fiber amplifier (EDFA). A narrowband filter of $\pm$12.5 GHz bandwidth is used to suppress the amplified spontaneous emission (ASE) from the EDFA. Then the optical pulses are launched into a $\sim$1450 m fiber via a circulator. The circulator also redirects the weak backscattered light into another EDFA for pre-amplification and another narrowband filter is used to suppress the ASE. Then the amplified light enters the IMZI scheme. Finally, three identical photodetectors are employed to acquire outputs of the scheme. It has to be noted that a short fiber is used here just to validate the functionality of the proposed method. The setup is essentially a standard φOTDR based on the IMZI scheme, whose sensing distance can reach tens of kilometers and is mainly limited by the fiber attenuation. Over 100 km sensing distance is possible if a proper signal amplification method is applied [29].

The optical frequency of the laser is scanned at 50 Hz. The pulse width is set as 10 ns and the pulse repetition rate is 20 kHz. One arm of the IMZI is 2 m longer than the other, determining the gauge length. The bandwidth of the photodetector is 125 MHz,

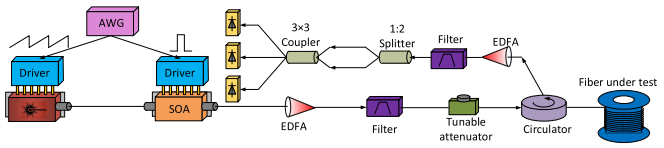

Fig. 4. Proposed φOTDR system that employs an optical frequency scanning laser and an imbalanced Mach–Zehnder interferometer.

which is large enough to faithfully acquire the backscattered light [30]. The analog signal from the photodetectors is digitalized at a rate of 250 MS/s. For the vibration measurement, a fiber section from ∼1401 m to ∼1412 m at the far-end is wrapped around a piezoelectric tube (PZT). The rest of the fiber is well protected during the measurement to avoid any unwanted environmental perturbation.

B. Results of the Phase Based φOTDR

The IMZI scheme in the proposed system realizes dynamic measurement up to 10 kHz, which is limited by the pulse repetition rate in the experiment. Moreover, the amplitude A_{de} is obtained during data processing, which will be used in the low frequency sensing based on ABM.

As expressed by (1), the obtained phase difference $\Delta\varphi$ is related to the optical frequency ν. At the perturbed part, the phase also changes due to the applied vibration. As a result, the phase measured at this range can be seen as a combination of a quasi-ramp wave at 50 Hz and a sinusoid wave at 1 kHz, as shown in Fig. 5(a). It is difficult to directly quantify the vibration amplitude from the shown curve. One method is to separate them in frequency domain. Since the laser scanning frequency is known, signals at any other frequencies are believed to originate from environmental changes and they can be easily filtered. A bandpass filter centered at 1 kHz with a width of 20 Hz is used to select the vibration signal and the filtered result is shown as a waterfall diagram in Fig. 8(a) in the supplement B.

The vibration measured in practice can have a broad and irregular frequency spectrum, unlike the vibration tested in lab, so it is difficult to determine the central frequency and width of the filter. Hence, a practical approach is to filter out the ramp signal at 50 Hz. Note that the signal also has harmonics at higher frequencies, which needs to be filtered out as well. In this case, a comb notch filter can be used. The filtered result is shown in Fig. 5(b), and is very similar to the phase obtained by a classical IMZI based φOTDR system without frequency scanning, displayed as dotted line in Fig. 5(b), validating that the proposed configuration can work as a standard phase based φOTDR system.

C. Results of the Amplitude Based φOTDR

This section demonstrates the φOTDR sensing based on cross correlation of the reflection spectra. As explained above, the

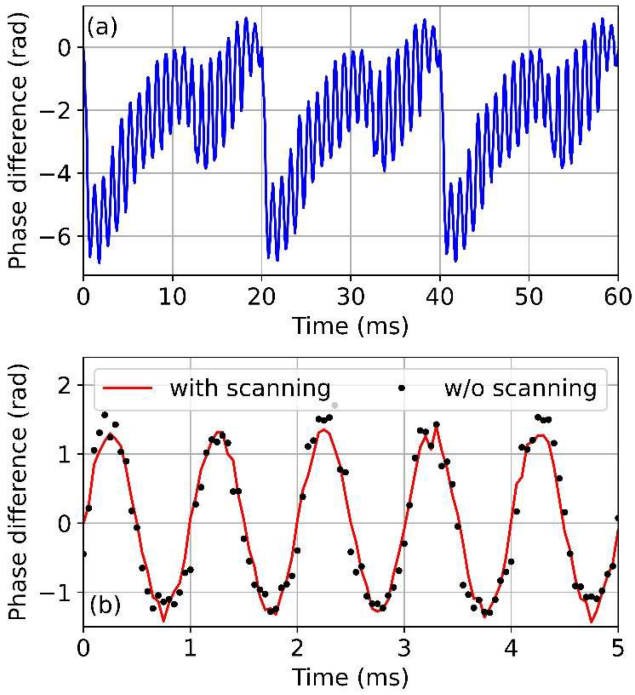

Fig. 5. (a) Optical phase demodulated at the perturbated fiber section. (b) Comparison of the filtered phase and the modified phase obtained by the φOTDR system based on the IMZI scheme with and without frequency scanning, respectively [13].

method requires frequency scanning, which limits the frequency response of the system from DC up to half of the scanning rate. The vibration frequency is thus adjusted to 2 Hz in this case, well below the upper limit of the measurable frequency that is 25 Hz. The discrete cross correlation is used to determine the spectral shift due to the non-linear frequency scanning.

The reflection spectrum at a given position can be plotted based on the demodulated amplitude A_{de}. The spectra at unperturbed (at 1394.98 m) and perturbed (at 1404.38 m) positions are shown in Fig. 6(a) and (b), respectively. The red spectra in both figures correspond to a measurement that is 120 ms later than the blue curve. At the unperturbed position, the interference condition is unmodified. Thus, the reflection spectrum remains the same, as shown by Fig. 6(a). The situation is however totally different at the perturbated part. Fig. 6(b) exhibits clearly a spectral shift due to the vibration of the PZT. In addition, the red reflection spectrum is distorted compared with the blue one, which has not been observed in the traditional ABM. The spectral distortion undermines the determination of the frequency shift. To minimize the negative impact, the pulse needs to be short and the scanning range to be small as mentioned in Section II-A.

To perform the DCC, the segment width is set as 3 MHz and the max lag of the frequency shift is 180 MHz. The blue curve shown in Fig. 6(c) is the correlation result of the spectra

$$CV\left(z,t\right)=\frac{\sum_{i=1}^{k}\left[A_{de}\left(z,t_0,\nu_i\right)-\bar{A}_{de}\left(z,t_0\right)\right]\cdot\sum_{i=1}^{g}\left[A_{de}\left(z,t,\nu_i\right)-\bar{A}_{de}\left(z,t\right)\right]}{\sigma\left[A_{de}\left(z,t_0,\nu_i\right)\right]\sigma\left[A_{de}\left(z,t,\nu_i\right)\right]} \tag{5}$$

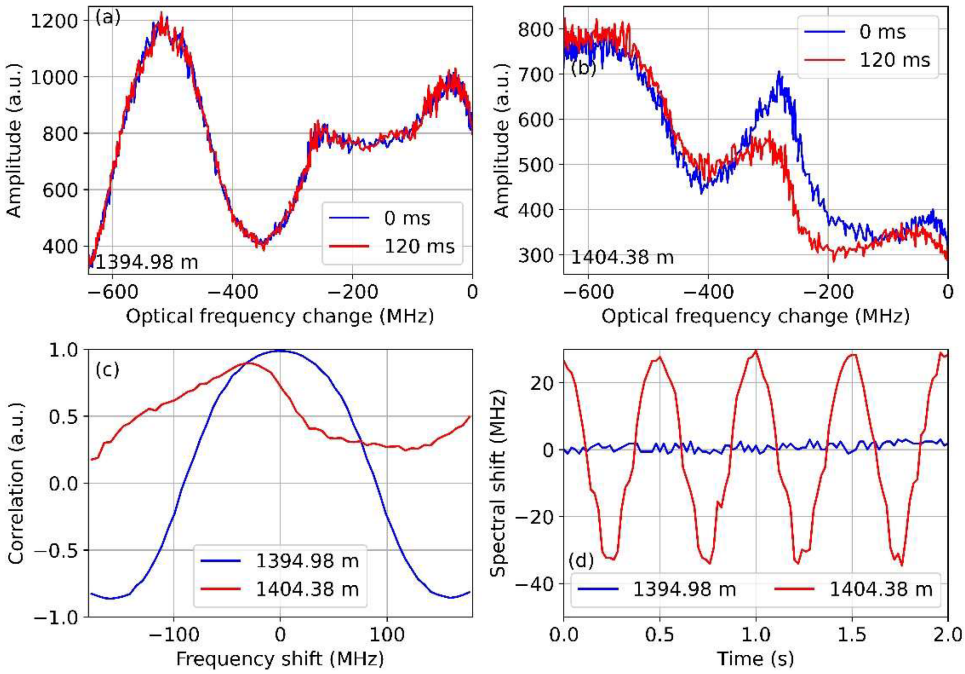

Fig. 6. Reflection spectra based on the demodulated amplitude at (a) unperturbed and (b) perturbated positions, (c) results of the discrete cross correlation of the spectra shown in (a) and (b), (d) the temporal profile of the spectral shifts at 1394.98 m and 1404.38 m.

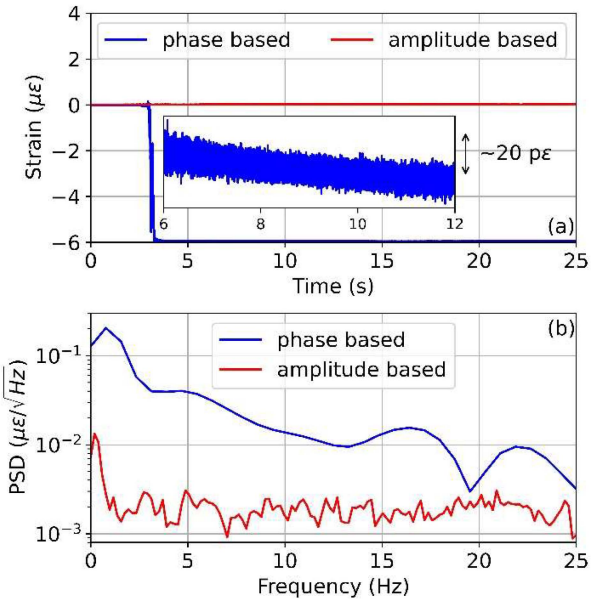

Fig. 7. Comparison of phase- and amplitude-based methods at an unperturbed fiber position. (a) Temporal evolution of the retrieved strain information, inset: zoom-in of the measured strain of the phase based method from 6 s to 12 s, (b) the corresponding power spectral densities of the measured strain.

at 1394.98 m, and its peak is at 0 MHz since this part of fiber experiences no environmental change. On the contrary, the DCC result within the vibrated fiber part peaks at a different frequency owing to the environmental perturbation. The peak is lower and less prominent due to the spectral distortion. The peak location of the correlation result reveals the spectral shift, which are plotted as a function of time in Fig. 6(d). The obtained shift varies slightly around 0 MHz at the unperturbed position, but it oscillates at 2 Hz due to the PZT vibration, validating the functionality of the amplitude-based method. To provide an overview, the result obtained around the perturbed section is plotted in a waterfall diagram in Fig. 8(b) in supplement B.

IV. Discussion

This section focuses on the comparison of the measurement results obtained by the ABM and PBM in the low frequency range. The result presented in the last section is reused here as for the amplitude-based sensing and a standard IMZI based φOTDR without frequency scanning provides the result of the phase-based sensing. The results are converted into strain based on the corresponding sensitivities (150 MHz/$\mu\varepsilon$ and 19.4 rad/$\mu\varepsilon$) for a straightforward comparison. Fig. 7(a) shows the temporal evolution of the strain obtained at an unperturbed fiber position by the two methods. The amplitude sensing provides a straight and thin line around 0 $\mu\varepsilon$ over 25 s, demonstrating a high quality measurement. On the other hand, the strain information obtained by the PBM exhibits large variations, particularly from 2 s to 4 s. Many spikes can be seen within this time slot, which are caused by the false phase unwrapping. The noise in the obtained phase can cause incorrect phase unwrapping, introducing an unnecessary phase offset of $\pm 2\pi$ to the unwrapped result [19]. The false unwrapping can occur several times during the measurement, as shown in Fig. 7(a), and the situation becomes even worse at the fading points. Due to the incorrect unwrapping, the baseline of the obtained strain is shifted to –6 $\mu\varepsilon$ after ~4 s. Besides the phase unwrapping error, the result suffers from a slow shift that is supposed to be induced by the random redistribution of the inhomogeneities in the boundary. The obtained strain increases

constantly from 6 s to 12 s by about 20 pε, as shown by the inset of Fig. 7(a). The PBM is consequently influenced by two more issues compared with the ABM. And these issues result in strong signal at low frequency, as shown in Fig. 7(b). The power spectral density (PSD) of the PBM is about 1 order-of-magnitudes higher than that of the ABM, making the PBS difficult to measure low frequency vibrations.

V. Conclusion

The simultaneous phase- and amplitude-based sensing methods have been experimentally realized by scanning the optical frequency of the laser in a standard IMZI based φOTDR system, so that the environmental variation can be quantified at multi-frequency bands. The PBM realizes vibration measurement at high frequency band. And the amplitude-based sensing, supported by the discrete cross correlation, delivers fading free and high-quality measurement at low frequency band from DC to half of the scanning rate. The measurement for both low and high frequencies is experimentally demonstrated. Such a feature matches perfectly the requirement of ground motion/movement monitoring.

The combination of PBM and ABM can also be realized based on many other traditional φOTDR systems, such as the one employs coherent detection, just by scanning the optical frequency of the laser. Furthermore, the combination enables various usages of the system, for example, temperature and strain discrimination can be realized based on the measured phase and the spectral shift. The potential of the proposed system will be explored in future work, for example to monitor gas storage caverns and nearby geological conditions.

Supplement

A. Detailed Analysis of the Phase Based φOTDR

The backscattered light from the fiber at position z can be expressed as $E(z, t) = A(z, t)e^{j\varphi(z, t)}$, where A and φ represent its amplitude and phase, respectively. The splitter in the IMZI scheme introduces a coefficient of $1/\sqrt{2}$ to the amplitude of the output light and a phase shift of $\pi/2$ between the two outputs. Likewise, the 3×3 coupler introduces a coefficient of $1/\sqrt{3}$ and a phase shift of $2\pi/3$ of its outputs [31]. Therefore, the optical field at the outputs of the IMZI can be expressed as

$$\begin{cases} E_1 = 1/\sqrt{6}\left[A(z)\, e^{j\phi(z)+j\pi/2} \right. \\ \qquad \left. + A(z+\Delta l)\, e^{j\phi(z+\Delta l)+j2\pi/3}\right] \\ E_2 = 1/\sqrt{6}\left[A(z)\, e^{j\phi(z)+j\pi/2} \right. \\ \qquad \left. + A(z+\Delta l)\, e^{j\phi(z+\Delta l)}\right] e^{j2\pi/3} \\ E_3 = 1/\sqrt{6}\left[A(z)\, e^{j\phi(z)+j\pi/2+j2\pi/3} \right. \\ \qquad \left. + A(z+\Delta l)\, e^{j\phi(z+\Delta l)}\right] \end{cases} \tag{6}$$

Note that the light propagating along the lower arm of the IMZI experiences a phase delay of $e^{j2\pi n\Delta l\nu/c}$ due to the longer fiber section. If the IMZI scheme is well isolated from environmental perturbations, this phase delay remains constant, so it is neglected in this paper.

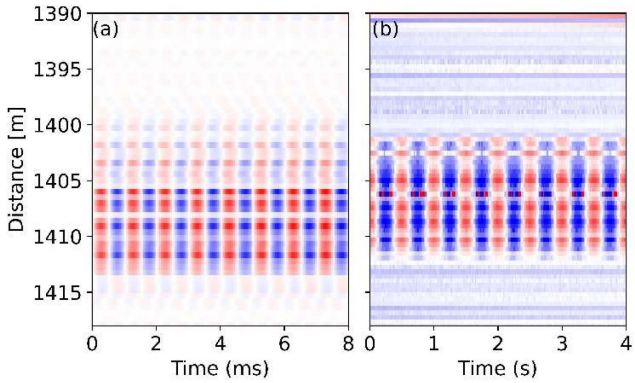

Fig. 8. Waterfall diagrams of the vibration measured by (a) phase-based method and (b) amplitude-based method.

The outputs of the IMZI are obtained by three identical photodetectors and the electrical signal can be expressed as $Pi = EiEi^*$. Therefore, P_1 can be written as

$$\begin{aligned} P_1(z) &= 1/6\left\{\begin{array}{l} A^2(z) + A^2(z+\Delta l) \\ -2A(z)\,A(z+\Delta l)\sin\left[\Delta\varphi(z) - 2\pi/3\right] \end{array}\right\} \\ &= P_{DC}(z) - P_{AC}(z)\sin\left[\Delta\varphi(z) - 2\pi/3\right] \end{aligned} \tag{7}$$

where $P_{\mathrm{DC}}(z) = [A^2(z) + A^2(z + \Delta l)]/6$ and $P_{\mathrm{AC}} = A(z)A(z + \Delta l)/3$. In the same way, P_2 and P_3 are obtained as:

$$\begin{aligned} P_2(z) &= P_{DC}(z) - P_{AC}(z)\sin\left[\Delta\varphi(z)\right] \\ P_3(z) &= P_{DC}(z) - P_{AC}(z)\sin\left[\Delta\varphi(z) + 2\pi/3\right] \end{aligned} \tag{8}$$

It is clear that the obtained signal is a function of the phase difference $\Delta\varphi$. For IQ demodulation, two orthogonal components must be found based on the signal. According to the basic trigonometric calculation, it turns out that

$$\begin{aligned} &-1/2P_1(z) + P_2(z) - 1/2P_3(z) = -3/2P_{AC}(z)\sin\left[\Delta\varphi(z)\right] \\ &-\sqrt{3}/2P_1(z) + \sqrt{3}/2P_3(z) = -3/2P_{AC}(z)\cos\left[\Delta\varphi(z)\right] \end{aligned} \tag{9}$$

As a result, the in-phase sig_I and quadrature sig_Q components are obtained as (2).

B. Overview of the Vibration Results Obtained by Both Methods

To provide the reader an overview, the results obtained by ABM and PBM around the vibrated section are plotted in Fig. 8 as waterfall diagrams. Obviously, both methods show a very similar perturbed position, but the PBM result exhibits a wider range. The phase difference $\Delta\varphi$ start to show the oscillation even when only one fiber position, either z or $z + \Delta l$, is subject to the vibration, which results in a wider perturbed range for the PBM.

References

[1] A. H. Hartog, *An Introduction to Distributed Optical Fibre Sensors*, 1st ed. Boca Raton, FL, USA: CRC Press, 2017.
[2] M. R. Fernández-Ruiz et al., "Distributed acoustic sensing for seismic activity monitoring," *APL Photon.*, vol. 5, no. 3, Mar. 2020, Art. no. 030901.

[3] T. Kiers et al., "Monitoring of an alpine landslide using dense seismic observations: Combining distributed acoustic sensing and 1000 autonomous seismic nodes," in *Proc. EGU 25th EGU Gen. Assem.*, 2023, p. EGU23-8986.
[4] S. Liehr, S. Münzenberger, and K. Krebber, "Wavelength-scanning coherent OTDR for dynamic high strain resolution sensing," *Opt. Exp.*, vol. 26, no. 8, pp. 10573–10588, Apr. 2018.
[5] Y. Koyamada, M. Imahama, K. Kubota, and K. Hogari, "Fiber-optic distributed strain and temperature sensing with very high measurand resolution over long range using coherent OTDR," *J. Lightw. Technol.*, vol. 27, no. 9, pp. 1142–1146, May 2009.
[6] M. R. Fernández-Ruiz, L. Costa, and H. F. Martins, "Distributed acoustic sensing using chirped-pulse phase-sensitive OTDR technology," *Sensors*, vol. 19, no. 20, Oct. 2019, Art. no. 4368.
[7] Z. Wang et al., "Coherent Φ-OTDR based on I/Q demodulation and homodyne detection," *Opt. Exp.*, vol. 24, no. 2, pp. 853–858, Jan. 2016.
[8] G. Tu, X. Zhang, Y. Zhang, F. Zhu, L. Xia, and B. Nakarmi, "The development of an Φ -OTDR system for quantitative vibration measurement," *IEEE Photon. Technol. Lett.*, vol. 27, no. 12, pp. 1349–1352, Jun. 2015.
[9] X. Lu, M. A. Soto, and L. Thévenaz, "Temperature-strain discrimination in distributed optical fiber sensing using phase-sensitive optical time-domain reflectometry," *Opt. Exp.*, vol. 25, no. 14, pp. 16059–16071, Jul. 2017.
[10] L. Zhang et al., "Distributed and dynamic strain sensing with high spatial resolution and large measurable strain range," *Opt. Lett.*, vol. 45, no. 18, pp. 5020–5023, Sep. 2020.
[11] X. Lu and K. Krebber, "Characterizing detection noise in phase-sensitive optical time domain reflectometry," *Opt. Exp.*, vol. 29, no. 12, pp. 18791–18806, Jun. 2021.
[12] Y. Wu et al., "Dynamic range enlargement of distributed acoustic sensing based on temporal differential and weighted-gauge approach," *J. Lightw. Technol.*, vol. 40, no. 9, pp. 3038–3045, May 2022.
[13] X. Lu, K. Hicke, and K. Krebber, "Approaching distributed ground motion sensing at high and low frequency ranges," in *Proc. 28th Int. Conf. Opt. Fiber Sensors*, 2023, Paper W4.18.
[14] P. Posey, G. A. Johnson, and S. T. Vohra, "Strain sensing based on coherent Rayleigh scattering in an optical fibre," *Electron. Lett.*, vol. 36, no. 20, pp. 1688–1689, Sep. 2000.
[15] A. Masoudi and T. P. Newson, "High spatial resolution distributed optical fiber dynamic strain sensor with enhanced frequency and strain resolution," *Opt. Lett.*, vol. 42, no. 2, pp. 290–293, Jan. 2017.
[16] A. Masoudi and T. P. Newson, "Analysis of distributed optical fibre acoustic sensors through numerical modelling," *Opt. Exp.*, vol. 25, no. 25, pp. 32021–32040, Dec. 2017.
[17] X. Lu, M. A. Soto, P. J. Thomas, and E. Kolltveit, "Evaluating phase errors in phase-sensitive optical time-domain reflectometry based on I/Q demodulation," *J. Lightw. Technol.*, vol. 38, no. 15, pp. 4133–4141, Aug. 2020.
[18] X. Lu and P. J. Thomas, "Numerical modeling of Fcy OTDR sensing using a refractive index perturbation approach," *J. Lightw. Technol.*, vol. 38, no. 4, pp. 974–980, Feb. 2020.
[19] H. Gabai and A. Eyal, "On the sensitivity of distributed acoustic sensing," *Opt. Lett.*, vol. 41, no. 24, pp. 5648–5651, Dec. 2016.
[20] X. Lu and K. Krebber, "Phase error analysis and unwrapping error suppression in phase-sensitive optical time domain reflectometry," *Opt. Exp.*, vol. 30, no. 5, pp. 6934–6948, Mar. 2022.
[21] X. Lu, M. A. Soto, and L. Thévenaz, "Impact of the fiber coating on the temperature response of distributed optical fiber sensors at cryogenic ranges," *J. Lightw. Technol.*, vol. 36, no. 4, pp. 961–967, Feb. 2018.
[22] J. K. Sahota, N. Gupta, and D. Dhawan, "Fiber Bragg grating sensors for monitoring of physical parameters: A comprehensive review," *Opt. Eng.*, vol. 59, no. 6, Jun. 2020, Art. no. 060901.
[23] M. Imahama, Y. Koyamada, and K. Hogari, "Restorability of rayleigh backscatter traces measured by coherent OTDR with precisely frequency-controlled light source," *IEICE Trans. Commun.*, vol. E91.B, no. 4, pp. 1243–1246, Apr. 2008.
[24] M. D. Mermelstein et al., "Rayleigh scattering optical frequency correlation in a single-mode optical fiber," *Opt. Lett.*, vol. 26, no. 2, pp. 58–60, Jan. 2001.
[25] S. Liehr et al., "Real-time dynamic strain sensing in optical fibers using artificial neural networks," *Opt. Exp.*, vol. 27, no. 5, pp. 7405–7425, Mar. 2019.
[26] K. Rehfeld, N. Marwan, J. Heitzig, and J. Kurths, "Comparison of correlation analysis techniques for irregularly sampled time series," *Nonlinear Processes Geophys.*, vol. 18, no. 3, pp. 389–404, Jun. 2011.
[27] R. A. Edelson and J. H. Krolik, "The discrete correlation function: A new method for analyzing unevenly sampled variability data," *Astrophys. J.*, vol. 333, pp. 646–659, Oct. 1988.
[28] D. R. S. Robertson, L. C. Gallo, A. Zoghbi, and A. C. Fabian, "Searching for correlations in simultaneous X-ray and UV emission in the narrow-line Seyfert 1 galaxy 1H 0707–495," *Monthly Notices Roy. Astronomical Soc.*, vol. 453, no. 4, pp. 3455–3460, Nov. 2015.
[29] L. D. van Putten, A. Masoudi, and G. Brambilla, "100-km-sensing-range single-ended distributed vibration sensor based on remotely pumped Erbium-doped fiber amplifier," *Opt. Lett.*, vol. 44, no. 24, pp. 5925–5928, Dec. 2019.
[30] X. Lu, M. A. Soto, L. Zhang, and L. Thévenaz, "Spectral properties of the signal in phase-sensitive optical time-domain reflectometry with direct detection," *J. Lightw. Technol.*, vol. 38, no. 6, pp. 1513–1521, Mar. 2020.
[31] T. Wang et al., "Comparison of amplitude-frequency response characteristics between DCM and Arctan algorithms in φ-OTDR," *J. Lightw. Technol.*, vol. 41, no. 20, pp. 6608–6614, Oct. 2023.